THE DEVELOPMENT OF NOVEL BEAM DIAGNOSTICS FOR LOW-MEV PROTONS

J.A. Bellesini*[1], J.S.L. Yap[1,2], A.F. Steinberg[1], S. Barg[1], S.L. Sheehy[1,3]
[1]The University of Melbourne, Melbourne, Australia
[2]Peter MacCallum Cancer Centre, Melbourne, Australia
[3]Australian Nuclear Science and Technology Organisation, Sydney, Australia

Abstract

A low-energy (0.5–3 MeV) demonstrator beamline for proton therapy is under development as part of the TURBO (Technology for Ultra-Rapid Beam Operation) project [1, 2]. In charged particle therapy, high energy layer switching times prolong beam delivery times, where beamlines with a large momentum acceptance (±42%) could alleviate this bottleneck and increase treatment efficiency. This beamline is being constructed for the University of Melbourne's Pelletron accelerator which operates at low energies and high current densities, requiring novel beam diagnostic instrumentation to monitor key parameters. We develop a pepper-pot mask method to measure the beam phase space distribution and quantify the emittance, and a multi-layer Faraday cup (MLFC) to measure the beam energy distribution, providing the adaptations required to operate under our experimental conditions. This work contributes to the development of a beam shaping section, and integration of a fixed-field, closed-dispersion beam transport section, toward demonstration of a proton beamline with the potential to shorten beam delivery times.

INTRODUCTION

A beam shaping section is required upstream of the large momentum acceptance beam transport section to modify the transverse distribution of the beam and to rapidly change the mean energy. This necessitates instrumentation and methods to be able to accurately measure and monitor fundamental parameters of the beam, including the transverse beam phase space and energy distribution. Pepper-pot masks are diagnostic devices used to measure the 4D transverse beam phase-space, commonly used for high-intensity particle beams at low-energies [3–6]. The operating principle of this technique is that a metal mask (e.g. steel, copper, tungsten) with a grid of holes of known size and spacing, intercepts the beam, splitting the incident beam into an array of smaller beamlets. These beamlets then travel over a known drift length to a scintillator screen or detector, where the pattern of beamlet spots is captured. This array of beamlets represent samples of the initial beam distribution, such that the analysis of the diverged beamlet pattern over this drift allows for an estimation of the beam position-angle phase space. From this, a statistical estimation of the emittance and Twiss (Courant-Snyder) parameters [7] to describe this elliptical distribution can then be acquired. While this technique is well established, only few studies have performed this method for low-MeV proton applications [8, 9].

A MLFC is a highly accurate diagnostic device which can measure the energy distribution of the proton beam [10–14]. The MLFC is constructed using conductive media segmented into multiple electrically isolated layers along the beam axis. When the beam is intercepted, charge is deposited and accumulates within each layer, where it can be measured independently to acquire a composite range distribution. Proton ranges are monotonic and strongly correlated with incident proton energy, thereby allowing direct beam energy determination from the measured charge distribution. This device provides benefits of minimal calibration requirements, compact form factor and robustness to high currents, compared to alternate methods of energy determination such as scintillation detectors or magnetic spectrometry [15, 16]. However, MLFCs available off-the-shelf are built for clinical energy ranges (70–250 MeV) and therefore are unsuitable for our experimental conditions with low-MeV protons. The adaptation to lower energies poses challenges on component design and construction, requiring the conductive material to be of lower stopping power or comprised of significantly thinner layers to achieve an energy resolution comparable to clinical systems. Due to this, MLFCs have not previously been implemented for this energy range.

PEPPER-POT MASK-BASED METHOD FOR MEASURING BEAM EMITTANCE

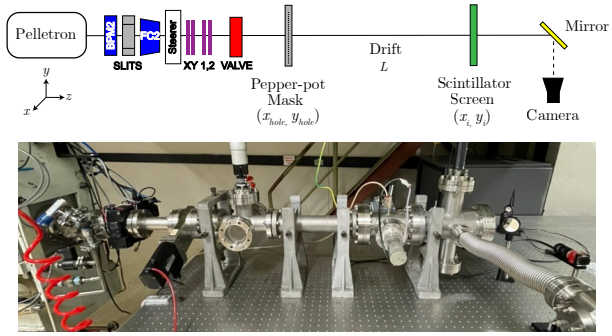

Figure 1: Pepper-pot experimental measurement. Diagram of apparatus (top), image of beamline (bottom).

Initial experimental work involving a pepper-pot based emittance measurement has been performed, showing the reconstruction of the full 4D transverse phase space of the proton beam generated by the University of Melbourne Pelletron accelerator (x, x' phase space is shown in Fig 2). We used a

* joel.bellesini@student.unimelb.edu.au

stainless steel pepper-pot mask with a grid consisting of 21 × 21 holes with 50 µm radius and 500 µm spacing. A proton beam with a mean energy of 3 MeV and current of approximately 10 nA was sent through the mask and onto a YAG:Ce scintillator screen [17], where the beamlet distribution pattern was imaged by a camera (CMOS sensor) positioned at 90° orthogonal to the beam axis using a high-reflectance silver coated mirror to reflect the beam off-axis (see Fig. 1). A peak detection algorithm was then implemented to first isolate the beamlets from the background signal via intensity thresholding, apply a data mask derived from known mask geometry (x_{hole}), and perform Gaussian fitting on each resolved beamlet to extract beamlet centroid position, angle and intensity (x_c, x_c', ρ), as well as per-beamlet position and angle distribution (x_i, x_i'). The root-mean-square emittance (ε_{RMS}) was then determined, representing a statistical estimation of area occupied by the beam in position-angle phase space, computed from the second-order moments.

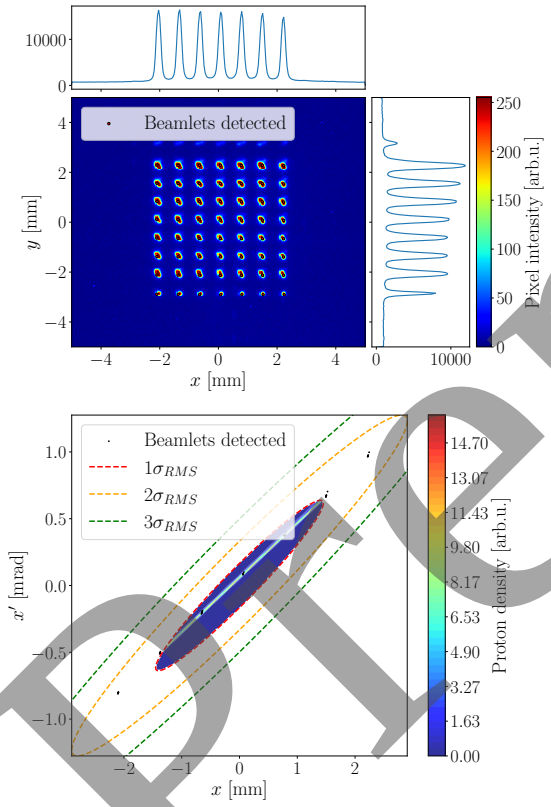

Figure 2: Pepper-pot camera image and beamlet detection (top). Phase space (x, x') reconstruction (bottom). Notably, the $1\sigma_{\text{RMS}}$ phase space ellipse appears to underestimate the emittance compared to other definitions ($2\sigma_{\text{RMS}}, 3\sigma_{\text{RMS}}$).

Table 1: Pepper-pot reconstructed parameters.

Parameter	Value	Error	Unit
ε_{RMS}	0.241	0.0144	mm · mrad
α	−3.710	0.221	
β	8.742	0.522	m
γ	0.001 69	1.01×10^{-4}	mm^{-1}

$$x_c' = \frac{x_c - x_{\text{hole}}}{L} \qquad \langle x^2 \rangle = \frac{\sum_{i=1}^{N} \rho_i x_c^2}{\sum_{i=1}^{N} \rho_i}$$

$$\langle x'^2 \rangle = \frac{\sum_{i=1}^{N} \rho_i x_c'^2}{\sum_{i=1}^{N} \rho_i} \qquad \langle x x' \rangle = \frac{\sum_{i=1}^{N} \rho_i (x_c x_c')}{\sum_{i=1}^{N} \rho_i}$$

$$\Sigma_{\text{centroids}} = \begin{pmatrix} \langle x_c x_c \rangle & \langle x_c x_c' \rangle \\ \langle x_c' x_c \rangle & \langle x_c' x_c' \rangle \end{pmatrix}$$

$$\Sigma_{\text{beamlet}} = \begin{pmatrix} \langle x_i x_i \rangle & \langle x_i x_i' \rangle \\ \langle x_i' x_i \rangle & \langle x_i' x_i' \rangle \end{pmatrix}$$

$$\varepsilon_{\text{RMS}}^2 = \det\left(\Sigma_{\text{centroids}} + \sum_{i=1}^{N} n_i \Sigma_{\text{beamlet}} \right)$$

The following equations are derived from the transfer matrix for a charged particle beam with a drift L, and are used to to compute Twiss parameters at the location of the mask [7]:

$$\beta(L) = \beta_0 - 2\alpha_0 L + \gamma_0 L^2$$

$$\alpha(L) = \alpha_0 - \gamma_0 L$$

$$\gamma(L) = \gamma_0$$

The parameter values and errors shown in Table 1 were derived using the above expressions (where $L = 0.745$ m, which is the distance of mask to screen). There are many errors encountered in a pepper-pot measurement, including beamlet width due to finite hole size and hole spacing (contributes to both x_i, x_i'), limited camera resolution (contributes to both x_i, x_i'), inherent beam variation and noise in measurement apparatus (contributes to ρ_i). Of these contributions, the hole size and spacing is assumed to be dominant, as the hole diameter imposes a physical limit to the achievable spatial and angular resolution of the system, where camera pixel size and electronic noise are comparatively small relative to the beamlet dimensions observed experimentally. In many pepper-pot measurement methods, this error is accounted for solely as a scalar term in the $\langle x'^2 \rangle$ definition. In this work, we choose to represent these error contributions rather using a per-beamlet (x_i) covariance matrix (Σ_{beamlet}) which is added to the centroid covariance matrix ($\Sigma_{\text{centroids}}$) in the form of a weighted average across all beamlets. It is from this resultant matrix where the root-mean-square emittance (ε_{RMS}) value is computed as the square-root of the determinant. This approach treats each beamlet as a finite phase space distribution rather than a point sample with an independently assigned angular uncertainty, thereby incorporating both positional and angular uncertainties, as well as their correlation, naturally weighted by the detected beamlet intensities. Consequently, this yields a more complete and physically representative estimation of the reconstructed beam emittance.

MULTI-LAYER FARADAY CUP FOR MEASURING BEAM ENERGY DISTRIBUTION

A prototype MLFC consisting of conductive layers of Aluminium foil (2.0 µm thick) is currently being constructed for proton beam energies from 0.5–3 MeV, with a projected mean resolution of 0.065 MeV. Many careful design considerations were taken due to the fine spatial and precision requirements imposed. For instance, the insulating material between conducting layers has been removed from the beam path through the implementation of an apertured PCB-based layer design. This configuration ensures that incident protons interact only with the conductive material, thereby improving the achievable proton energy resolution. The overall detector design, including material selection, was informed through analysis of stopping power and projected range data for a broad range of conductive materials from the National Institute of Standards and Technology (NIST) PStar tables [18], in conjunction with Monte Carlo simulations performed using TOPAS [19], and 3D component modelling conducted using CAD software (Fusion 360) [20].

Aluminium foil (99.1% purity, 100 mm × 100 mm × 2.0 µm) was sub-divided into 49 (7 × 7 grid) composite layers (12 mm × 12 mm × 2.0 µm) using a UV–laser cutter (355 nm). For each layer, a PCB (0.25 mm thick) was designed and fabricated with contact points for each layer to be bonded, allowing accumulated charge to be grounded and detected as a current. A thicker, side-plate PCB (1.3 mm thick) has also been designed for the dual purpose of passage of electrical signals from each layer PCB, and to add structural integrity to the layer stack. The layer geometry and electronic schematic designs were performed using Fusion 360 [20] and KiCad [21], respectively. This yields a total height of 4 cm when 48 layers stacked, where parallel-plate capacitance is sufficiently low for our temporal requirements (68 pF). Each channel passes through a transimpedance amplifier for low-bias, low-noise amplification, tuned to detect nA level currents as mV output voltages, over a 1 MΩ resistor. A trio of (16:1) multiplexers scan through 48 signals with an anticipated temporal resolution of 1–5 Hz per channel (sufficient for our use case). Finally, an Arduino Nano is used for analog-to-digital conversion, multiplexer controlling, and readout to a computer. The PCBs and ultra-low profile surface mount device (SMD) electrical components have been externally manufactured for the construction of an initial prototype, and internal manufacturing of in-vacuum housing components are required for future experimental validation.

In order to experimentally test this device, an energy reconstruction algorithm is required to interpret the detected signals. The layer composition and stopping power tables are used to correlate detected ranges to initial energies. A few corrections are required to accurately perform this reconstruction. These include accounting for scattering and straggling effects, which lead to a reconstructed energy distribution that is both broadened and systematically shifted towards lower energies. This arises from stochastic variations in energy loss as well as angular deviations in particle trajectory as the beam propagates through the layers. This reconstruction has been simulated and is shown over a range of proton energies in Fig. 3. This plot demonstrates accurate reconstruction of initial beam energies and verifies our design provides sufficient energy resolution for our purposes.

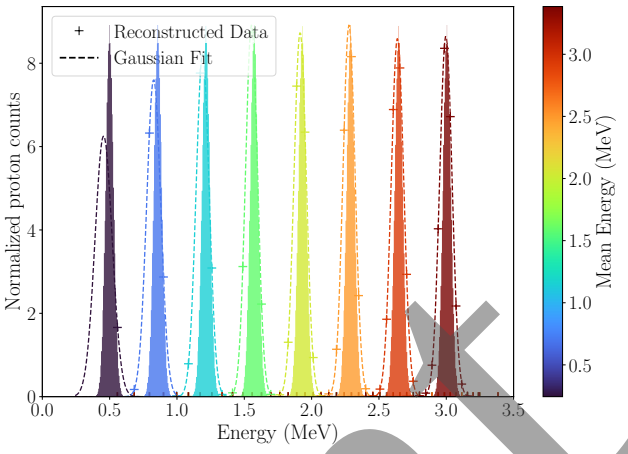

Figure 3: Reconstructed proton beam energy distribution from simulation data (using TOPAS, 10^8 histories per run). Initial energy distributions shown as histograms, reconstructed distributions shown as scattered crosses fitted with dashed lines.

CONCLUSION

Here we have described the design and development of beamline diagnostics under novel conditions, consisting of a pepper-pot mask for beam emittance measurement and an MLFC for beam energy measurement. These are being constructed for use in a scaled-down large momentum acceptance beam delivery system for proton therapy, where both diagnostics have been adapted for low-MeV proton beams. This custom-built suite of diagnostic instrumentation may provide a potential solution across many fields of research within accelerator physics, material science such as PIXE [22], aerospace engineering to study cosmic radiation damage on microelectronics [23], or radiobiological studies investigating cellular reaction to radiation [24]. Future work will involve further prototyping, optimisation of reconstruction scripts, introduction of live control and readout systems, and integration with the beam shaping and transport section for TURBO.

ACKNOWLEDGEMENTS

We acknowledge the facilities and the scientific and technical assistance provided by the Heavy Ion Accelerators (HIA) node at the University of Melbourne. HIA is supported by the Australian Government through the National Collaborative Research Infrastructure Strategy programme. The authors also thank S. Gregory, A. Saint, T. Bonin and J. McCallum for technical support and Pelletron resources. J. S. L. Yap is generously supported by the Gross Foundation.

REFERENCES

[1] J. S. Yap, A. F. Steinberg, S. J. Clarke, H. X. Norman, R. B. Appleby, and S. L. Sheehy, "Progress Toward TURBO: A Novel Beam Delivery System for Charged Particle Therapy", *Journal of Physics: Conference Series*, vol. 2687, no. 9, p. 092004, Jan. 2024. doi:10.1088/1742-6596/2687/9/092004

[2] A. F. Steinberg, R. B. Appleby, J. S. L. Yap, and S. L. Sheehy, "Design of a large energy acceptance beamline using fixed field accelerator optics", *Physical Review Accelerators and Beams*, vol. 27, no. 7, p. 071601, Jul. 2024. doi:10.1103/PhysRevAccelBeams.27.071601

[3] O. Apsimon, B. Williamson, and G. Xia, "A numerical approach to designing a versatile pepper-pot mask for emittance measurement", *Nuclear Instruments and Methods in Physics Research Section A: Accelerators, Spectrometers, Detectors and Associated Equipment*, vol. 943, p. 162485, Nov. 2019. doi:10.1016/j.nima.2019.162485

[4] F. Osswald *et al.*, "Transverse emittance measurement in 2D and 4D performed on a Low Energy Beam Transport line: benchmarking and data analysis", *Journal of Instrumentation*, vol. 18, no. 01, P01011, Jan. 2023. doi:10.1088/1748-0221/18/01/P01011

[5] J. Pitters *et al.*, "Pepperpot emittance measurements of ion beams from an electron beam ion source", *Nuclear Instruments and Methods in Physics Research Section A: Accelerators, Spectrometers, Detectors and Associated Equipment*, vol. 922, pp. 28–35, Apr. 2019. doi:10.1016/j.nima.2018.12.072

[6] D. Marx *et al.*, "Single-shot reconstruction of core 4D phase space of high-brightness electron beams using metal grids", *Physical Review Accelerators and Beams*, vol. 21, no. 10, p. 102802, Oct. 2018. doi:10.1103/PhysRevAccelBeams.21.102802

[7] B. J. Holzer, "Introduction to Transverse Beam Dynamics", en, Apr. 2014, doi:10.5170/CERN-2013-007.27, https://arxiv.org/abs/1404.0923v1 (visited on 05/06/2026),

[8] H. R. Kremers, J. P. M. Beijers, and S. Brandenburg, "A pepper-pot emittance meter for low-energy heavy-ion beams", *Review of Scientific Instruments*, vol. 84, no. 2, p. 025117, Feb. 2013. doi:10.1063/1.4793375

[9] T. Nagatomo, V. Tzoganis, M. Kase, O. Kamigaito, and T. Nakagawa, "Development of a pepper-pot emittance meter for diagnostics of low-energy multiply charged heavy ion beams extracted from an ECR ion source", *Review of Scientific Instruments*, vol. 87, no. 2, 02B920, Nov. 2015. doi:10.1063/1.4934688

[10] C. Kunert, J. Bundesmann, T. Damerow, A. Denker, and A. Weber, "A Multi-Leaf Faraday Cup especially for proton therapy of ocular tumors", pp. 2149–2152, 2014.

[11] P. L. Yeap *et al.*, "Proton Beam Range and Charge Verification Using Multilayer Faraday Collector", *Technology in Cancer Research & Treatment*, vol. 23, p. 15330338241262610, Jul. 2024. doi:10.1177/15330338241262610

[12] K. P. Nesteruk *et al.*, "Measurement of the Beam Energy Distribution of a Medical Cyclotron with a Multi-Leaf Faraday Cup", *Instruments*, vol. 3, no. 1, Jan. 2019. doi:10.3390/instruments3010004

[13] B. Tesfamicael *et al.*, "Use of commercial multilayer Faraday cup for offline daily beam range verification at the McLaren Proton Therapy Center", *Medical Physics*, vol. 46, no. 2, pp. 1049–1053, 2019.

[14] C. Makowski, M. Deutsch, C-Stefan. Schmitzer, and A. Schüller, "Multileaf Faraday cup for beam energy verification in radiation therapy with ultra-high dose-rate electron beams and ion beams", *Medical Physics*, vol. 53, no. 3, e70362, Mar. 2026. doi:10.1002/mp.70362

[15] U. Schneider and D. Renker, "Proton energy measurements using a NaI(T1) scintillator", *Nuclear Instruments and Methods in Physics Research Section A: Accelerators, Spectrometers, Detectors and Associated Equipment*, vol. 388, no. 1-2, pp. 199–203, Mar. 1997. doi:10.1016/S0168-9002(97)00349-5

[16] P. Häffner, C. Belver Aguilar, S. Braccini, P. Scampoli, and P. A. Thonet, "Study of the Extracted Beam Energy as a Function of Operational Parameters of a Medical Cyclotron", *Instruments*, vol. 3, no. 4, p. 63, Dec. 2019. doi:10.3390/instruments3040063

[17] V. Sipala *et al.*, "YAG(Ce) crystal characterization with proton beams", *Nuclear Instruments and Methods in Physics Research Section A: Accelerators, Spectrometers, Detectors and Associated Equipment*, vol. 654, no. 1, pp. 349–353, Oct. 2011. doi:10.1016/j.nima.2011.07.008

[18] NIST, "Stopping-Power & Range Tables for Electrons, Protons, and Helium Ions", *NIST*, Oct. 2009. https://www.nist.gov/pml/stopping-power-range-tables-electrons-protons-and-helium-ions

[19] B. Faddegon *et al.*, "The TOPAS tool for particle simulation, a Monte Carlo simulation tool for physics, biology and clinical research", *Physica Medica*, vol. 72, pp. 114–121, Apr. 2020. doi:10.1016/j.ejmp.2020.03.019

[20] Autodesk Inc., "Fusion 360", 2026, https://www.autodesk.com/products/fusion-360/overview (visited on 05/06/2026),

[21] KiCad Developers, "KiCad EDA", 2026, https://www.kicad.org/ (visited on 05/06/2026),

[22] K. Ishii, "PIXE and Its Applications to Elemental Analysis", *Quantum Beam Science*, vol. 3, no. 2, p. 12, Jun. 2019. doi:10.3390/qubs3020012

[23] V. Kraus, M. F. Garcia, L. Menzio, and M. Moll, "Proton Energy Dependence of Radiation Induced Low Gain Avalanche Detector Degradation", en, Feb. 2026, https://arxiv.org/abs/2602.01800v1 (visited on 05/10/2026),

[24] S. Zonitsas *et al.*, "Development and Evaluation of a Proton Irradiation Setup for Radiobiological Studies Using Low-Energy Protons with a Polyenergetic Spectrum (0–5.5 MeV, Mean 4.1 MeV)", *Radiation*, vol. 6, no. 1, p. 7, Mar. 2026. doi:10.3390/radiation6010007